Digital holographic microscopy for automated 3D cell identification: an overview

(Invited Paper)

Arun Anand[1] **and Bahram Javidi**[2*]

[1]*Applied Physics Department, Faculty of Technology and Engineering, The M.S. University of Baroda, Vadodara 390001, India*

[2]*Department of Electrical and Computer Engineering, U-2157, University of Connecticut, Storrs, CT 06269-2157, USA*

[*]*Corresponding author: bahram@engr.uconn.edu*

Received February 25, 2014; accepted April 4, 2014; posted online May 30, 2014

Digital holographic (DH) microscopy is a promising technique for quantitative phase contrast imaging. It provides complex amplitude of the object wavefront, which in turn yields the thickness distribution of the object. An added advantage of the technique is its ability for numerical focusing, which provides the thickness distribution of the object at different axial planes. In this invited paper, we present an overview of our reported work on two beam DH microscopyto acquire different cell parameters for cell imaging and automated cell identification. Applications to automated monitoring of stem cells without destroying the cells and automated identification of malaria infected red blood cells are discussed.

OCIS codes: 090.1995, 180.6900, 120.5050, 170.1530.

doi: 10.3788/COL201412.060012.

1. Introduction

In imaging of living cells, resolution as well as contrast is necessary to study and evaluate the dynamic processes occurring in them. But many of the biological specimens are transparent to visible light. For these objects, bright field microscope provides only low contrast intensity images and a single object plane. Staining of the specimen can improve the contrast, but this may cause an alteration of the cells. These objects may produce a change to the phase of the probe beam, that is, the beam interacting with the object, due to spatially varying optical thickness. Thus, phase contrast imaging techniques will be better suited for cellevaluation. The phase of the probe beam is very sensitive to the optical thickness mismatch between the cytoplasmic content of the cells and the surrounding medium. This phase change can be used to construct high contrast images of the specimen[1,2]. If access to the phase of the object wavefront is available, optical thickness profile of the specimen can be reconstructed, leading to quantitative phase microscopy (QPM). Digital holographic (DH) microscopy is such a technique, which provides three dimensional (3D) optical thickness profiles of transparent specimen[3−15]. In DH microscopy, holograms or interference patterns are recorded on image sensors and reconstructed using numerical methods by simulating the process of diffraction from these structures[3,4]. This reconstruction provides the complex amplitude of the object wavefront, which in turn provides the object phase information and hence the thickness profile. An added advantage of DH microscopy is its ability of numerical focusing, which provides a way by which different object planes can be brought to focus during the reconstruction process. Comparison of the object phase with any other phase distribution becomes possible in the case of DH microscopy. Thus, reconstructing the phase distribution with and without the object and then interferometricaly comparing them, the distortions due to the aberrations in the optical system may beremoved and phase information due to the object alone can be obtained[11−15]. Also, using a series of holograms the time evolution of the cell morphology could be studied[11−13]. We are involved in the development of applications using DH microscopy for quantitative imaging of cells. In this invited paper, we present an overview of our reported and published research in the area of DH microscopywith applications in the imaging of cells for their parameter extraction, comparison and automated identification[8,10,11,14,15].

2. Overview of DH microscope

A sketch of the DH microscope used in some of our investigations is shown in Fig. 1(a)[11−15]. It uses He-Ne laser as the source although a variety of other coherent or partially coherent sources may be used. The beam from the source is split into two. One of the beams acts as the reference beam. The other beam is allowed to pass through the object under investigation. The object is magnified using an appropriate microscope objective (selection of the objective lens depends upon the required magnification and resolution). The object under investigation is mounted on a translation stage for easy focusing. The object and reference beams are made to interfere at the detector plane or the plane of the hologram at an angle in off-axis geometry by employing Mach-Zehnder interferometer configuration. A CCD array records the holograms, that is, the interference pattern.The detector is located near the image plane of the objective lens. To match the curvatures of the wavefronts at the detector plane, an objective of the same configuration as the one used for magnification was introduced in the reference arm of the setup. Figure 1(b) shows the portion inside the dotted rectangle shown in Fig. 1(a), depicting the magnification and interference process. The distance (d) between the hologram and the image plane is also shown.

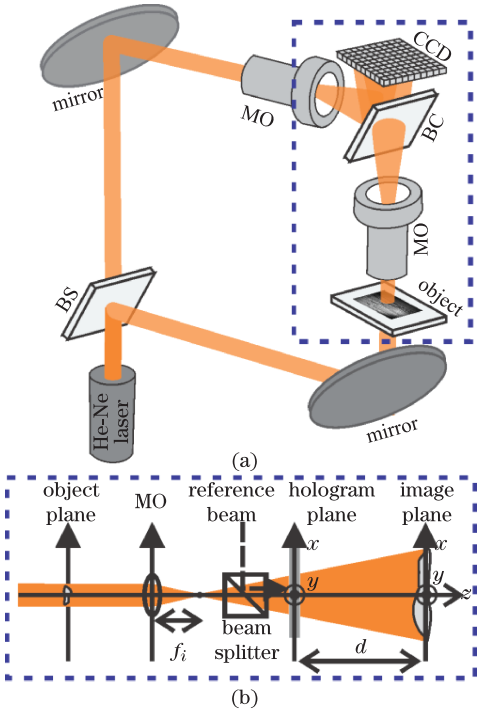

Fig. 1. (Color online) (a) DH microscope; (b) magnification of the object and interference of the object and reference beams.

For each set of object holograms recorded with cells present in the field of view, a reference hologram, containing only the surrounding medium in the field of view, was also recorded. Digital holograms are reconstructed numerically by simulating the scattering of the reference beam from the interference pattern. It involves the use of diffraction integrals, which describes the propagation of wavefronts between parallel planes. The recorded digital holograms are discrete in nature, therefore, they have finite pixel and array sizes, and a discrete form of the diffraction integral is used. Either the Fresnel–Kirchhoff diffraction integral or the angular spectrum propagation (ASP) integral could be used for numerical reconstructions[11−15]. Both of these approaches describe the scattering of the reference wave by the hologram and the selection of the reconstruction integral depends upon the particular application. In the case of transparent or phase objects, like living cells, which do not scatter light appreciably and for small propagation distances, the angular spectrum approach, which does not have any restriction on propagation distance, is more appropriate. For quantitative microscopy of phase objects, the ASP approach also makes compact experimental setup possible. Another advantage of this method is that it separates out the different diffracted components in the frequency space and hence there will not be an overlap between the beams in the image plane[12,16]. Here, ASP integral is used for cell reconstructions. Complex amplitude of the reconstructed wavefront at the image plane, which is at a distance d from the hologram plane according to ASP integral is[17]

$$U(x,y,d) = \int_{-\infty}^{\infty}\int \bar{U}(f_X,f_Y;0)\,G(f_X,f_Y,d) \cdot e^{i2\pi(f_X x+f_Y y)}\mathrm{d}f_X\mathrm{d}f_Y, \quad (1)$$

where $\bar{U}(f_X,f_Y;0)$ is the filtered angular spectrum of the scattered reference wavefront at the hologram plane, $G(f_X, f_Y, d)$ is the free space propagation function, and f_X and f_Y are the spatial frequencies in the x and y directions respectively. The intensity of the wavefront at the image plane is the square of the absolute value of the complex amplitude and is given by

$$I(x,y,d) = |U(x,y,d)|^2. \quad (2)$$

The phase of the object wavefront is the angle that the complex amplitude makes with the real axis and is given by

$$\varphi(x,y,d) = \arctan\frac{Im[U(x,y,d)]}{Re[U(x,y,d)]}. \quad (3)$$

The phase which is obtained from holograms without the object, but with the surrounding medium present in the field of view is subtracted from the phase obtained from the holograms with the object present in the field of view to yield the phase difference $\Delta\phi(x, y)$. This phase difference is related to the refractive index of the cell n_C, refractive index of the surrounding medium n_R and the thickness of the cell $L(x, y)$ at a time instance through

$$\Delta\varphi(x,y,t) = \frac{2\pi}{\lambda}(n_C - n_R)\,L(x,y,t). \quad (4)$$

The advantage of computing the phase difference is that, it nullifies the effects due to aberrations in the optical system and brings out the phase information due to the object alone. Using Eq. (4), one can calculate the thickness distribution of the cell, provided the constant refractive index of the cell and the surrounding medium are available. If the refractive index values are not available, Eq. (4) can be used to compute the optical thickness (refractive index × thickness) distribution.

3. Some examples of imaging of cells

The holographic microscope was first used to examine onion skin cells[12]. A thin slice of onion skin was mounted on a microscope slide and images using a 10×(NA=0.25) microscope objective lens were obtained. An 8-bit CCD camera with 4.65-μm pixel pitch was used for recording the holograms. The image plane was located 5 mm from the CCD plane. Reconstructions of the hologram were achieved using an in-house developed reconstruction and analysis software. The angular spectrum of the object was selected using a rectangular window from the Fourier transform of the complex amplitude at the hologram plane. Figure 2(a) shows the reconstructed phase contrast image of the object. Figure 2(b) is the optical thickness profile of the onion skin calculated after unwrapping of phase map in Fig. 2(a) and using Eq. (4) (see Ref. [12]).

4. Automatic identification of malaria infected red blood cells

The holographic microscope has been used for automatic discrimination of malaria infected red blood cells (RBC) in a thin blood smear[14]. In Asia and Africa, malaria is one of the most widespread and potentially fatal disease. Correct diagnosis of malaria is essential for its medication and cure. In developing countries, the main clinical diagnostics of malaria is based on microscopic inspection of stained blood smears by a trained technician.

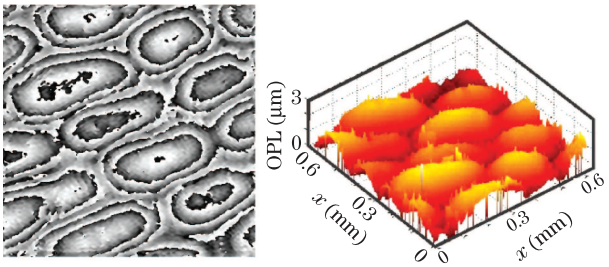

Fig. 2. (Color online) (a) Wrapped phase distribution obtained for onion skin cells; (b) optical thickness profiles of onion skin cells obtained from unwrapped phase distribution.

But visual identification of malarial RBCs may become unreliable due to lack of sufficiently trained technicians, poor quality microscopes and bio-chemical inspection. So a field portable compact and low cost instrument that can automatically discriminate between RBCs could be beneficial in these circumstances.In Ref. [14], we used DH microscopy for automatic identification of malaria infected RBCs by comparing the shape profiles computed from the phase profile. A correlation algorithm was used to discriminate between the shapes of the cells and determines whether the cell is infected by malaria. Figure 1 shows the DH microscope used in investigating RBCs using a low power coherent source. Here also a He-Ne laser source operating at 611nm was utilized with the experimental geometry shown in Fig. 1(a). A microscopic objective (oil immersion, 100×, NA=1.25) magnifies the object. Same CCD as in the previous experiment was used. Blood samples were collected from healthy individuals and from individuals detected with severe malaria. These samples were centrifuged to separate malaria infected RBC. Thin blood smears were formed on glass slide and they were covered with a cover slip. Both object (with RBCs present in the field of view) and reference (with blood plasma present in the field of view) were recorded.For RBCs a constant refractive index (n_C) of 1.42 and for the surrounding medium (plasma) a constant refractive index (n_R) of 1.34 was used to convert the phase information into the thickness information. Figure 3(a) shows the obtained thickness profile of a healthy RBC after phase subtraction[14].

Before identification, the location of the cells in the thin smear was determined by thresholding the obtained thickness profile with the standard deviation of the background thickness profile (Fig. 3(b)). The type of the RBC, that is, healthy or malaria infected was then identified by finding the correlation between the cell shapes at different axial planes as shown in Fig. 4[14]. The obtained phase contrast images of healthy RBC and malaria infected RBC at different axial planes is shown in Fig. 5[14].

In the experiments, 43 healthy and malaria infected RBC were used. Firstly, the shape of healthy RBCs was compared to other healthy RBCs and an average correlation value was obtained. In the second step, the shape of healthy RBC was compared with that of malaria infected RBC and the average for this was also obtained. The average of the correlation coefficient from shape comparisons of healthy-healthy and healthy-malaria cell pair was used as the discriminating parameter for cell identification. Figure 6 shows the correlation coefficient for different cell combinations[14]. The correlation coefficients were determined by using shape data from 20 axial planes. A threshold value of 0.88 provided the highest probability of correct classification. False positive and false negative rates of the technique were 1.1 out of 10 and 1.6 out of 10, respectively.

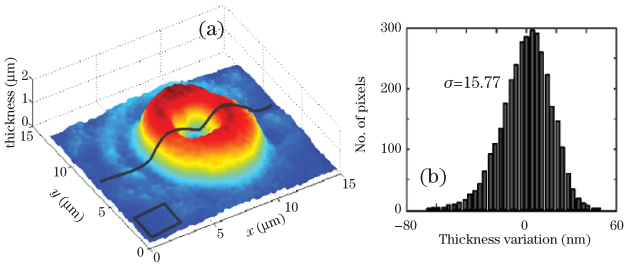

Fig. 3. (Color online) (a) Obtained thickness distribution for a healthy red blood cell. (b) Histogram of thickness variation of the background shown inside the rectangle in (a).

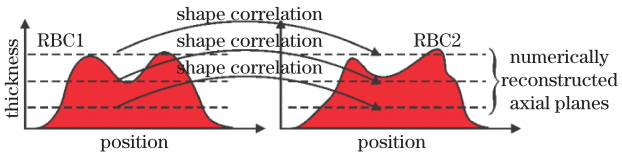

Fig. 4. (Color online) Concept of cell identification using thickness profile at different axial planes.

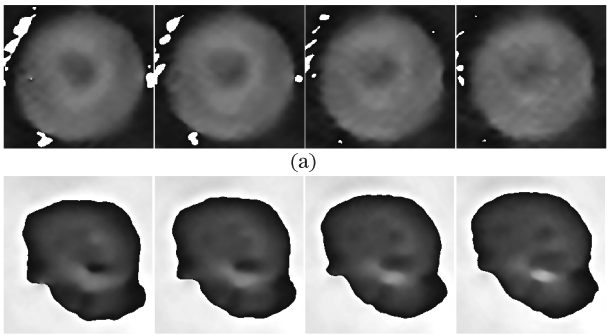

Fig. 5. Phase contrast images of (a) healthy RBC and (b) malaria infected RBC obtained at various axial distances. Distance between successive axial planes is 0.72 μm.

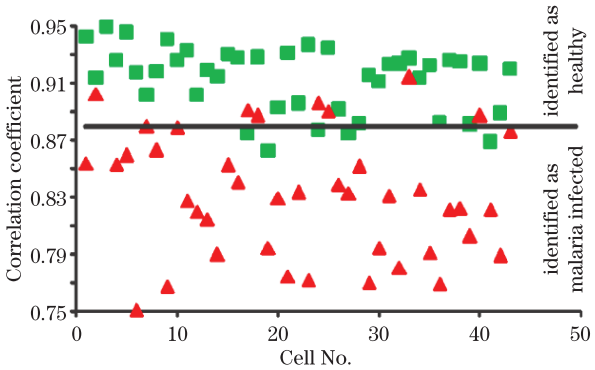

Fig. 6. (Color online) Average correlation coefficient from shape comparison of different cell pairs using data from 20 axial planes plane (Healthy, Malaria infected, —— threshold).

Integration of DH microscopy and statistical algorithms such as simple correlation algorithms has potential to be used as an automaticdetection technique that can discriminate between different classes of RBCs. In Ref. [14], a comparison between the shapes of the test cell with the database of healthy and malaria infected cells provided information on whether the cell is healthy or not.

5. Imaging stem cell dynamics

Embryonic stem cells (ESCs) are very important for the development of cell-based therapeutic strategies[11,13]. One of the most important evaluation parameter for ESC is their visualization in various states of differentiation. But presently no method is available to evaluate live cells in culture and determine their phenotype. A characterization technique, to distinguish ESC in culture as undifferentiated stem cells, fate-restricted progenitor cells or differentiated mature cells, is needed. Most of the currently used methods require that the cells in culture be 'fixed' with paraformaldehyde - killing the cells - so that specific proteins in the cell can be analyzed using antibodies with fluorescent tags for identification. Standard bright field microscopy has weaknesses as we discussed earlier. Cell sorting technique can also be used, which involves removing the cells from their growth conditions and passing them through a laser-guided 'sorter' into a collection vial and then back to the Petri dish. Unfortunately, no method exists that allows full phenotypic evaluation of cultured ESCs without disrupting their established culture environment. DH microscope can be used to provide spatio-temporal evolution of cell morphology and so might be an ideal tool for investigation of stem cells for their imaging, parameter extraction, and identification. In Ref. [13], we investigated the use of DH microscope for imaging the growth of ESC. For this investigation we used an inverted setup, in which the object was imaged by an objective lens placed below the glass slides containing the cells. Inverted setup allows use of large magnification, large numerical aperture and short working distance microscope objectives without the need for immersion. R1-669 mouse ESCs were used in the experiments. Holograms of the ESC colonies were obtained at 24 hour intervals for 4 days. These holograms were used to compute the optical path length (OPL) distribution of the ESC colony at each time instance (using Eq. (4)). The OPL distributions were used to compute mainly four parameters pertaining to the cell colony, namely,i) lateral dimensions, ii) area, iii) optical thickness, and iv) optical volume of the specimen. Figure7(a) shows the wrapped phase distribution for a day 2 colony of ESCs[11,13]. Figure7(b) is the unwrapped phase map, which is used for determination of OPL distribution.

Figure8 shows the change in 3D OPL distribution of the colony with time. Growth of the colony laterally and axially is quite visible[11,13].

Binary image obtained after thresholding OPL distribution with the mean OPL in the area where there is no cell was used to determine lateral growth of the colony. Both the change in lateral dimension and area of the ESC colony were computed. Figure 9 shows the time variation of lateral dimension and area of the colony, showing a steady growth with time[13].

From the reconstructed thickness profile, the axial growth of the colony can also be calculated. Change in the optical thickness profile along the x and y direction with time is shown in Fig. 10[13]. Since the area represented by each reconstructed pixel as well as the thickness

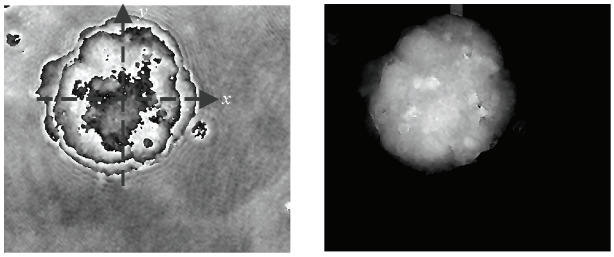

(a) (b)

Fig. 7. (a) Wrapped phase distribution for a day 2 ESC colony. (b) Unwrapped phase distribution obtained using Goldstein's branch cut method.

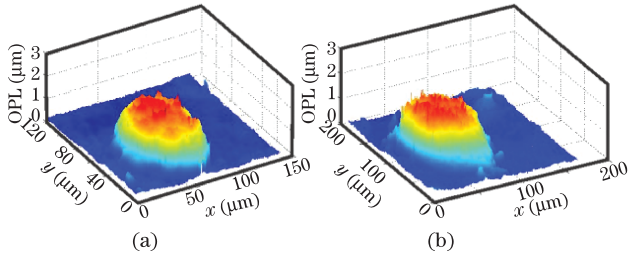

Fig. 8. (Color online) Optical thickness profiles of ESC colonies on (a) day 2 and (b) day 3.

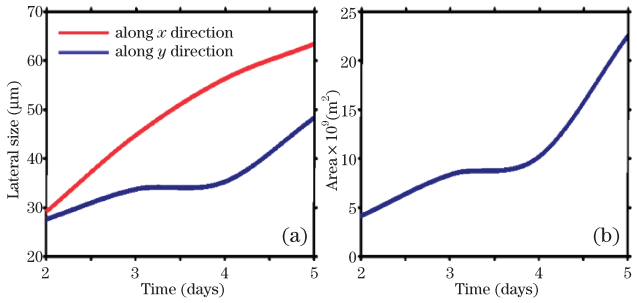

Fig. 9.(Color online) Time evolution of (a) lateral dimension and (b) area of the stem cell colony.

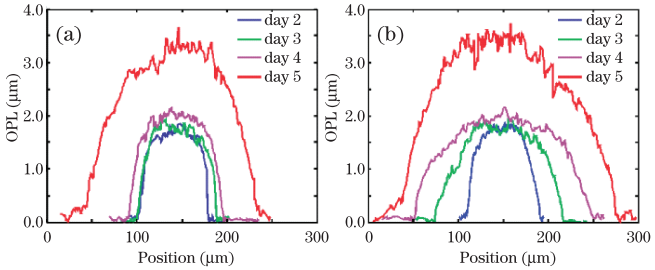

Fig. 10. (Color online) Time evolution of thickness profile of the stem cell colony (a) along x direction and (b) along y direction.

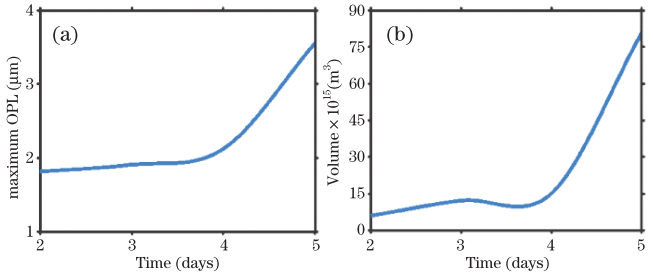

Fig. 11. (Color online) (a) Axial evolution of the stem cell colony in terms of maximum OPL and (b) temporal evolution of optical volume.

at each pixel are available, optical volume of the cell colony can be computed. Figure 11(a) shows the change in maximum optical thickness as a function of time[13]. This increase also reflects as an increase in volume of the colony also, which is shown in Fig. 11(b).

From Figs. 8 to 11, it can be summarized that the axial growth of the colony exponentially increases after day 4. The area occupied by the colony as well as its volume also increase rapidly after day 3. It indicates rapid lateral and axial expansion of the colony. This axial expansion, due to stacking of more stem cells along the axial direction, cannot be visualized using conventional microscope. So the 3D visualization and measurement approach using DH microscope can be used to analyze details of ESC and monitor their profiles throughout the differentiation process and the cell proliferation rate.

6. Cell sorting

DH microscopy can be used to get information from different object layers by using its numerical focusing capability. We have used this capability for sorting of stem cells and fibroblast cells (FBCs) in a mixture[15]. The reconstructed complex amplitude of the probe wavefront was used along with statistical identification to distinguish between ESCs and FBCs. Figure 12 shows the phase contrast images as well as thickness profiles of ESC as well as FBCs, obtained from holograms containing the particular class of cells only[15].

Before identification of the cells, their locations were determined by thresholding with the background OPL. The 3D thickness data of the cells has a complex structure. The complex data of each cell is extracted at 100 axial planes by numerical focusing. The successive axial planes were separated by 0.1 μm and 100 pixels are randomly sampled from each plane of the cell. The data collection process is shown in Fig. 13[15].

For each image pixel, a four dimensional vector of the complex magnitude and the location information of the pixel is recorded. Thus, each cell is consisting of multiple sets (planes) of observations. Since one cannot assume that the distributions at different axial planes to be same, observations from different planes cannot be pooled together. Thus, proper feature extraction algorithms are required before any clustering algorithm can be applied on the 3D image data. We applied a nonparametric statistical method based on entropy estimation technique to reduce the structure of 3D image data to features with smaller dimensions[15]. The data after transformation can be shown mathematically to be asymptotically normally distributed, so that the transformed data for each cell can asymptotically be seen as from a mixture of normal distributions. The standard clustering algorithms such as the model-based clustering algorithms, which are

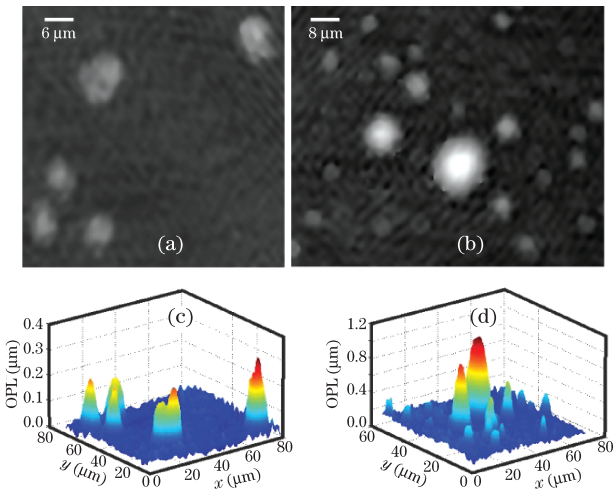

Fig. 12. (Color online) (a) Phase contrast image obtained for ESCs and (b) FBCs; Thickness distribution of (c) ESCs and (d) FBCs.

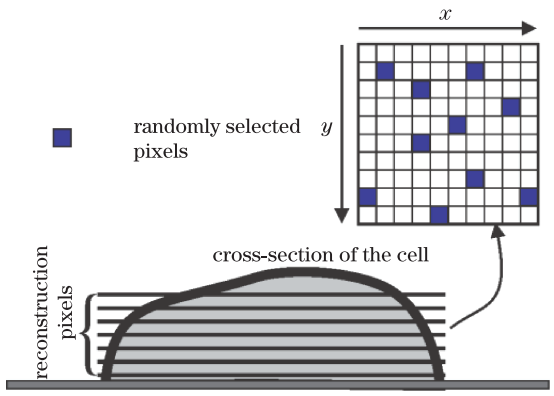

Fig. 13. (Color online) Reconstructed image planes of a cell and the process of data collection.

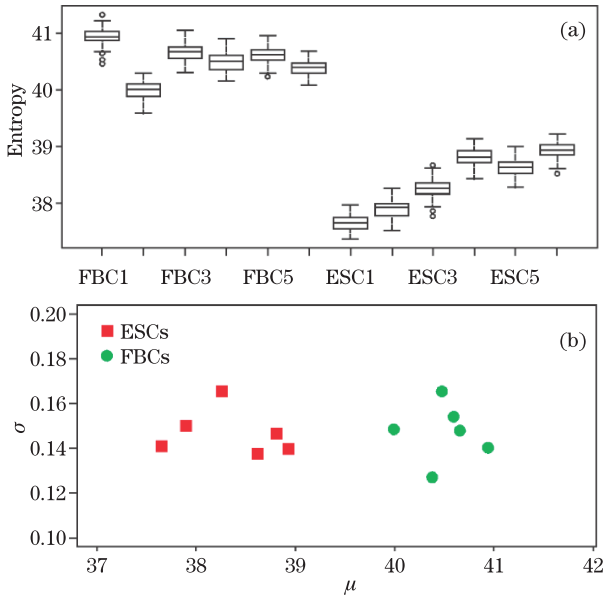

Fig. 14. (Color online) (a) Box-plots of the negative entropy values estimates, (b) Fitted parameters (μ_i, σ_i) of the negative entropy estimates.

based on the assumption of normal mixtures, can easily be applied to the transformed data to further extract the feature vectors for each cell. 6 ESCs and 6 FBCs were used in the analysis. Figure 14 shows the classification results, based on the negative entropy of the distribution[15].This method does not rely on any parametric assumptions and provides an efficient procedure for the utilization of model-based clustering and linear discriminant methods in the discriminant analysis of stem cells.

7. Conclusions

In conclusion, we present an overview of our reported research for applications of two-beam DH microscopy for cell imaging applications. This imaging modality can be used for thickness profiling of cells and their automated identification. It can be useful in identification of diseases, feature extraction of cells, dynamic imaging of cells as well as cell sorting. The main drawback of two beam DH microscope setup is its low temporal stability, especially without proper vibration isolation.

This might be a hurdle when submicron level cell fluctuations are to be measured. Presently we are working on self-referencing two beam setups[18−20], which would give us information on the sub-micrometer level cell fluctuations along with all the other advantages of the two-beam setup described in this paper.

While this paper overview some of our own reported work on the subject of automated cell identification, there are a variety of other approaches to automated cell identification using holographic microscopy which have been reported[21−23]. Also, other holographic techniques may be used for recording information about the cells[24−29] followed by a variety of algorithms for cell identification[30−33].

8. Acknowledgement

We would like to acknowledge the financial assistance from UGC through major research grant 42-776/2013(SR) and DAE-BRNS research grant 2013/34/11/BRNS/504.

References

1. F. Zernike, Physica **9,** 686 (1942).
2. G. Nomarski, J. Phys. Radium **16**, 9 (1955).
3. T. Kreis, *Handbook of Holographic Interferometry* (Wiley-VCH, Weinheim, 2005).
4. U. Schnars and W. Jueptner, *Digital Holography: Digital Hologram Recording, Numerical Reconstruction and Related Techniques* (Springer, Berlin, 2005).
5. T. Zhang and I. Yamaguchi, Opt. Lett. **23,** 1221 (1998).
6. E. Cuche, F. Bevilacqua, and C. Depeursinge, Opt. Lett. **24,** 291 (1999).
7. P. Marquet, B. Rappaz, P. J. Magistretti, E. Cuche, Y. Emery, T. Colomb, and C. Depeursinge, Opt. Lett. **30,** 468 (2005).
8. B. Javidi, I. Moon, S. Yeom, and E. Carapezza, Opt. Express **13,** 4492 (2005).
9. B. Kemper, A. Bauwens, A. Vollmer, S. Ketelhut, P. Langehanenberg, J. Muthing, H. Karch, and G. von Bally, J. Biomed. Opt. **15,** 036009 (2010).
10. D. Shin, M. Daneshpanah, A. Anand, and B. Javidi, Opt. Lett. **35,** 4066 (2010).
11. I. Moon, M. Daneshpanah, A. Anand, and B. Javidi, Opt. Photon. News **22,** 18 (2011).
12. A. Anand, V. Chhaniwal, and B. Javidi, IEEE J. Disp. Technol. **6,** 500 (2010).
13. A. Anand, V. K. Chhaniwal, and B. Javidi, IEEE Photon. J. **3,** 546 (2011).
14. A. Anand, V. K. Chhaniwal, N. Patel, and B. Javidi, IEEE Photon. J. **4,** 1456 (2012).
15. R. Liu, A. Anand, D. K. Dey, and B. Javidi, J. Opt. Soc. Am. A (in press) (2014).
16. S. De Nicola, A. Finizio, G. Pierattini, P. Ferraro, and D. Alfieri, Opt. Express **13,** 9935 (2005).
17. J. W. Goodman, *Introduction to Fourier Optic s*(McGraw-Hill, New York, 1996).
18. A. S. G. Singh, A. Anand, R. A. Leitgeb, and B. Javidi, Opt. Express **20,** 23617 (2012).
19. V. K. Chhaniwal, A. S.G. Singh, R. A. Leitgeb, B. Javidi, and A. Anand, Opt. Lett. **37,** 1527 (2012).
20. A. Anand, P. Vora, S. Mahajan, V. Trivedi, V. Chhaniwal, A. Singh, R. Leitgeb, and B. Javidi, Pramana–J. Phys. **82,** 71 (2014).
21. A. ElMallahi, C.Minetti, and F. Dubois, Appl. Opt. **52,** A68 (2013).
22. E. A. Ozcan and U. Dmirci, Lab. Chip.**8,** 98 (2008).
23. I. K. Moon and B. Javidi, J. R. Soc. Interface **4,** 305 (2007).
24. Y. Frauel, T. Naughton, O. Matoba, E. Tahajuerce, and B. Javidi, Proc. IEEE **94,** 636 (2006).
25. V. Mico, J. Garcia, Z. Zalevsky, and B. Javidi, Opt. Lett. **34,** 1492 (2009).
26. F. Dubois, L. Joannes, and J.-C. Legros, Appl. Opt. **38,** 7085 (1999).
27. Y. Zhang, G. Pedrini, W. Osten, and H. J. Tiziani, Opt. Lett. **29,** 1787 (2004).
28. B. Javidi and E. Tajahuerce, Opt. Lett. **25,** 610 (2000).
29. D. Kim and B. Javidi, Opt. Express **12,** 5539 (2005).
30. B. Javidi and D. Painchaud, Appl. Opt. **35,** 318 (1996).
31. P. Refregier, V. Laude, and B. Javidi, Opt. Lett. **19,** 405 (1994).
32. B. Javidi and J. Wang, J. Opt. Soc. Am. A **11,** 2604 (1994).
33. M. Hollander and D. A. Wolfe, *Nonparametric Statistical Methods* (Wiley, New York, 1999).